RSC Advances

Solvothermal synthesis of graphene-BiOCl0.75Br0.25 microspheres with excellent visible-light photocatalytic activity

Journal:	*RSC Advances*
Manuscript ID:	RA-ART-02-2015-002852.R1
Article Type:	Paper
Date Submitted by the Author:	26-Mar-2015
Complete List of Authors:	Yuan, Xingzhong; Hunan University, College of Environmental Science and Engineering Liu, Yang; Hunan University,, Wang, Hou; Hunan University,, Chen, Xiaohong; Central South University, Gu, Shansi; Hunan University,, Jiang, Qian; Hunan University,, Wu, Zhibin; Hunan University,, Jiang, Longbo; Hunan University,, Zeng, Guangming; Hunan University,,

Solvothermal synthesis of graphene-$BiOCl_{0.75}Br_{0.25}$ microspheres with excellent visible-light photocatalytic activity

Yang Liu [a, b], Xingzhong Yuan [a, b *], Hou Wang [a, b], Xiaohong Chen [c], Shansi Gu [a, b], Qian Jiang [a, b], Zhibin Wu [a, b], Longbo Jiang [a, b], Guangming Zeng [a, b]

[a] College of Environmental Science and Engineering, Hunan University, Changsha 410082, PR China

[b] Key Laboratory of Environment Biology and Pollution Control, Hunan University, Ministry of Education, Changsha 410082, PR China

[c] School of Business, Central South University, Changsha 410083, PR China

[*] Corresponding author at: College of Environmental Science and Engineering, Hunan University, Changsha 410082, PR China. Tel.: +86 731 88821413; fax: +86 731 88823701.

E-mail address: yxz@hnu.edu.cn (X.Z. Yuan)

Abstract

Three-dimensional $BiOCl_{0.75}Br_{0.25}$/graphene (BG) microspheres have been synthesized via a facile solvothermal route. The as-prepared samples were characterized by powder X-ray diffraction (XRD), field emission scanning electron microscopy (FESEM), X-ray Photoelectron Spectroscopy (XPS), UV-vis diffuse reflectance spectra (UV-vis DRS) and Brunauer-Emmett-Teller (BET) area. The photocatalytic activities of the samples were evaluated by the degradation of Rhodamine B (RhB) under visible light irradiation. It was shown that the BG photocatalysts with 5.0 wt% graphene (BG5.0) exhibited the highest photocatalytic activity, which was almost up to 2.3 times than that of pure $BiOCl_{0.75}Br_{0.25}$. The enhanced photoactivity of BG5.0 was mainly attributed to the effective light absorption, the larger specific surface areas and the more efficient charge transportations and separations.

Keywords

Reduced graphene oxide; $BiOCl_{0.75}Br_{0.25}$; RhB; photocatalytic degradation

Introduction

Recently, organic dyes are extensively used to color products in the textile industry (nylon, wool, cotton, and silk) as well as for varnish, waxes, plastics and *etc*. Since many N-containing dyes such as RhB are resistant to conventional chemical and biological treatment, semiconductor-based photocatalysis captures great interest as a kind of "green" technology for degrading toxic pollutants[1, 2]. Among numerous semiconductors, bismuth oxyhalides have been extensively studied due to their cheap and environmental properties. The highly anisotropic layered structure can also efficiently induce the separation of photo-generated electron-hole pair [3-6]. Recently, the coalescence of semiconductors concerned BiOX (X = Cl, Br, I) with apposite band potentials turned out to be an attractive approach for the enhancement of pure BiOX. Coupled semiconductor systems such as BiOI/BiOBr[7], BiOCl/BiOBr[8], TiO_2/BiOX[9, 10], Bi_2S_3/BiOCl[11], N/BiOBr[12] and Ag/BiOBr[13] have been reported to have higher photocatalytic activity than that of the individual semiconductor. Besides, bismuth oxyhalides-based alloyed compounds containing more than one type of halogen, namely $BiOCl_xI_{1-x}$[14] , $BiOBr_xI_{1-x}$[15], and $BiOCl_xBr_{1-x}$ [16] are also certified to be effective photocatalysts for the degradation of pollutants under visible light irradiation. For example, Jia *et al*. successfully prepared $BiOBr_xI_{1-x}$ by a simple solvothermal and the $BiOBr_{0.2}I_{0.8}$ microspheres possessed the best photocatalytic activity under visible light irradiation. Kima *et al*. found that the flower-like 3D-structure $BiOCl_xI_{1-x}$ synthesized in ethylene glycol (EG) owned better adsorption and photocatalytic performance than that of the stacked 2D plate-like structures. Generally, the photocatalytic activity of

the hybrids is superior to the monomer. Unfortunately, the fast recombination of photo-generated charge carriers still limits the application of the photocatalysts. Therefore, increasing carbon materials as electron transport matrices are employed in retarding the recombination of electron-hole species.

Currently, carbon black, activated carbon, carbon nanotubes and graphite are found to occupy a vital position in heterogeneous catalysis as either catalysts or catalyst supports[17]. Graphene, a new carbon material with a monolayer of sp^2-hybridized carbon atoms, has drawn much attention due to its large specific surface area, high carrier mobility and superior chemical stability. Our previous review has summarized the recent advances of the graphene-based hybrids for the decontamination of wastewater and researched the absorbability for the heavy metal and organic dyes[18-20]. The specifically two-dimensional conjugated structure also guarantees its usage as a supporting platform to disperse and stabilize semiconductors for potential applications in catalysis[21-27].

In the present study, we firstly realized the complex of $BiOCl_{0.75}Br_{0.25}$ and graphene to improve the photocatalytic activity of $BiOCl_{0.75}Br_{0.25}$ via a facile one-pot solvothermal method. The samples were characterized by FESEM, XPS and UV-vis DRS. The highly photocatalytic activities of BG with different amounts of graphene were evaluated by the degradation of RhB. The by-products in aqueous solution after photocatalytic reaction were further analyzed by high-performance liquid chromatography (HPLC). Finally, a feasible mechanism for the degradation of RhB on BG systems was proposed.

2. Experimental

2.1 Preparation of $BiOCl_{0.75}Br_{0.25}$/graphene composites

All of the reagents were of analytical grade and used without any further purification. RhB was obtained from Tianjin Kemiou Chemical Reagent Co., Ltd (Tianjin, China). Graphene oxide (GO) was synthesized from natural graphite powder according to the modified Hummers method described in our previous report[19]. Firstly, a set of $BiOCl_xBr_{1-x}$ were straightforwardly prepared by controlling the initial molar ratio of hexadecyl trimethyl ammonium chloride (CTAC) and hexadecyl trimethyl ammonium bromide (CTAB) in the preparation protocol. The preliminary experiment confirmed that the $BiOCl_xBr_{1-x}$ exhibited the highest photocatalytic activity at x = 0.75. Thus, various BG microspheres with different contents of graphene were prepared. In a typical synthesis, 3.0 mmol of $Bi(NO_3)_3 \cdot 5H_2O$ was dissolved into 40.0 mL of ethylene glycol (EG). Then, CTAC and CTAB with a total molar amount of 3 mmol were added to the previous solution. Meanwhile, different mass GO was dispersed in EG by sonication and then added to the reacted-mixture. The mixture was poured into a 100ml Teflon-lined stainless steel autoclave and maintained at 160°C for 10 h, and then cooled to room temperature naturally. The precipitate was collected by centrifugation, washed with deionized water and anhydrous ethanol. Finally, the products were dried under vacuum at 80 °C. The $BiOCl_{0.75}Br_{0.25}$ /graphene samples with 2.0, 5.0, 10.0 wt. % of graphene, were labeled as BG2.0, BG5.0 and BG10.0, respectively.

2.2 Catalysts characterization

The surface morphologies of the prepared samples were characterized by a field emission scanning electron microscopy (FESEM) (JSM-7001F, Japan). The X-ray diffraction (XRD) patterns were obtained with Bruker AXS D8 Advance diffractometer using Cu-K*a* source (λ = 1.541 Å). The surface elemental composition analyses were conducted based on the X-ray Photoelectron Spectroscopy spectra (XPS) (Thermo Fisher Scientific, UK). UV-visible diffuse-reflectance spectra (UV-vis DRS) of the samples were recorded using a Varian Cary 300 spectrometer outfitted with an integrating sphere. The Brunauer-Emmett-Teller (BET) specific surface area and pore size of the samples were measured with an automatic instrument (ASAP2020, Micromeritics, USA).

2.3 Photocatalytic test and analysis

The photocatalytic activities of the as-obtained samples were evaluated by the degradation of RhB under visible light irradiation. Typically, 50 mg of the photocatalyst was suspended in a 150 mL of RhB aqueous solution (50 mg/L). Prior to irradiation, the suspension was stirred for 1 h in the dark to attain adsorption-desorption equilibrium. The reactor was then exposed to a 500 W Xe lamp (CHF-XM500, Beijing) equipped with a UV cutoff filter ($\lambda \geq 420$ nm) with magnetic stirring. At specific time intervals, 4 mL suspensions were sampled and centrifuged at 8000 rpm for 5 min to remove the photocatalyst powder. The concentration of RhB was determined based on the absorption at 554 nm using a UV-vis spectrophotometer. The HPLC analyses were performed using Agilent 1100 HPLC instrument system equipped with UV-VIS detector. The system used a C_{18} inversed phase column and

the column temperature was set at 25℃. The mixture of methanol and H_2O (7:3) was used as mobile phase with the flow rate of 0.8 mL/min.

3. Results and discussion

3.1 Characterization of the catalyst

The purity and crystallinity of the as-prepared samples were confirmed by XRD technique and were depicted in Fig. 1. All the diffraction peaks for x=0.0 and 1.0 were readily indexed to the structure of the BiOBr (JCPDS card No. 09-0393) and BiOCl (JCPDS card No. 06-0249) respectively. In addition, the diffraction peaks of $BiOCl_xBr_{1-x}$ shift gradually to larger angles with increasing x values, which demonstrated that there was no separated phase and nucleation of BiOBr or BiOCl in the formation of alloyed $BiOCl_{0.75}Br_{0.25}$ microspheres.[28-30] It was worth-noting that no apparent peaks of GO were observed in $BiOCl_{0.75}Br_{0.25}$/graphene samples, implying that the GO was almost reduced under the hydrothermal conditions. However, the main peak assigned to reduced graphene oxide (RGO, $2\theta = 26^{\circ}$) may be overlapped with the peak of tetragonal BiOCl at 25.8 °[17]. In addition, it may also due to the low amount and relatively weak diffraction intensity of graphene in the composite.

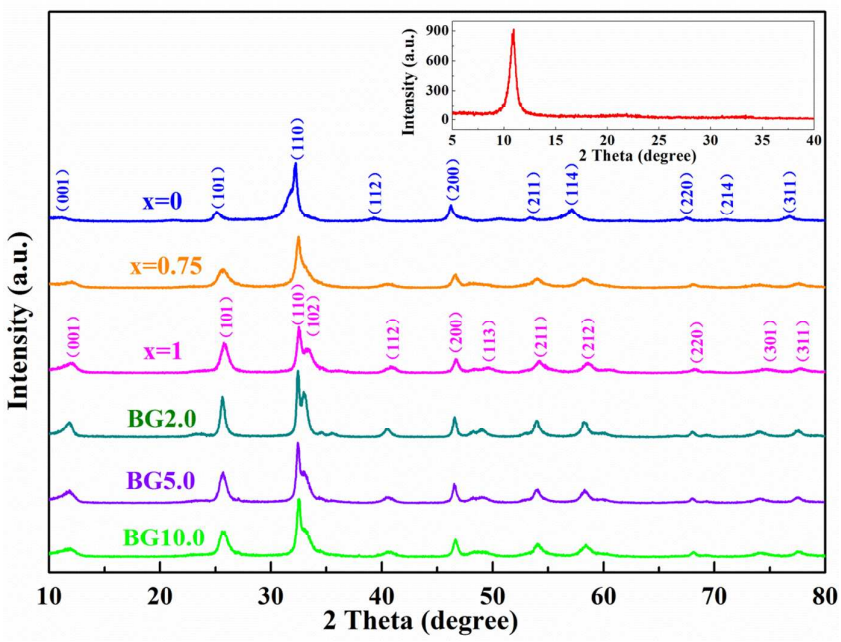

Fig.1. XRD patterns of GO, BiOBr, $BiOCl_{0.75}Br_{0.25}$ BiOCl and $BiOCl_{0.75}Br_{0.25}$/graphene (BG2.0, BG5.0, BG10.0) samples.

The morphology of the samples was determined by FESEM and the typical images were delineated in Fig. 2a-b. Clearly, the pristine $BiOCl_{0.75}Br_{0.25}$ exhibited lots of scattered microspheres with the diameters of around 3-4 μm (Fig. 2a). The morphology of the $BiOCl_{0.75}Br_{0.25}$ and BG5.0 samples was further investigated by TEM. As can be clearly seen in Fig. 2b and Fig.2e, the RGO displayed intrinsic microscopic wrinkles and owned a well-defined layered structure. The microspheres of $BiOCl_{0.75}Br_{0.25}$ were randomly distributed on both sides of the graphene sheets, exhibiting strong chemical interactions with the RGO sheets. The HRTEM image showed the characteristic lattice fringes of $BiOCl_{0.75}Br_{0.25}$ in the graphene nanosheets matrix (Fig. 2f). The lattice spacing was calculated to be 0.322 nm. Moreover, the EDX spectrum of the BG5.0 sample showed the presence of Bi, O, Br, Cl and C

elements, confirming the formation of $BiOCl_{0.75}Br_{0.25}$/graphene composites. The elemental mapping of the BG5.0 sample was also presented in Fig.S1.

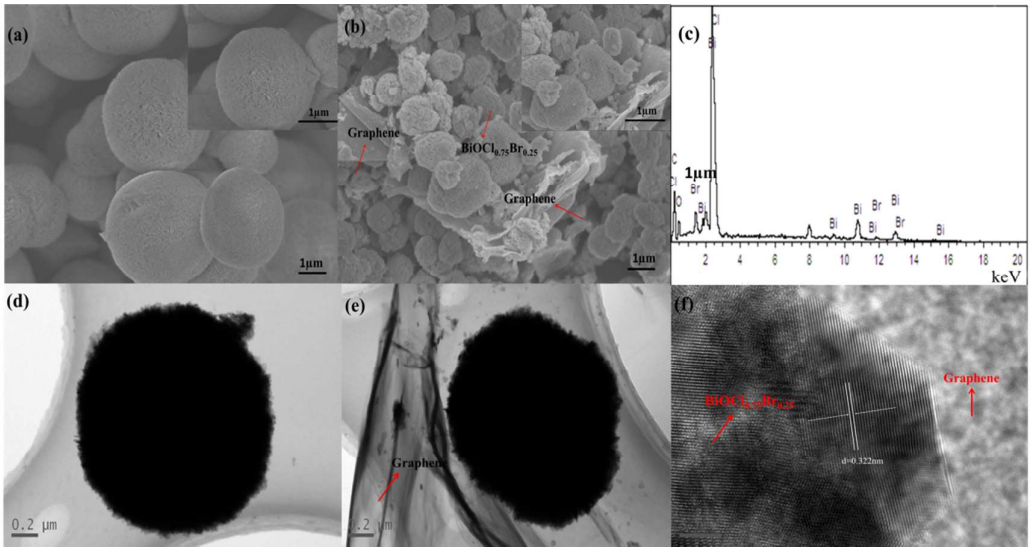

Fig.2. FESEM and TEM image of (a, d) $BiOCl_{0.75}Br_{0.25,}$ (b, e) BG5.0, (c) the EDX spectrum of BG5.0 and HRTEM (f) image of BG5.0.

The XPS analysis of BG5.0 powder was further performed for the measurement of surface compositions and chemical states of the sample (Fig. 3). The survey XPS spectrum revealed that the BG5.0 composites were composed of Bi, O, Cl, Br, and C (Fig. 3a). A high-resolution Bi 4f spectrum in Fig. 3b showed that the bands located at binding energies of 164.74 and 159.44 eV were assigned to the Bi 4f S = 5/2 and 7/2 spin-orbital splitting photoelectrons in the $BiOCl_{0.75}Br_{0.25}$ chemical state[31]. Apart from the two characteristic peaks, two other weak peaks centered at 164.01 and 158.43 eV were found, which may arise from the Bi-C bond on the film surface of graphene [31, 32].The Br 3d peak associated with the binding energy at 68.92 eV (Fig. 3c) can be ascribed to Br^- in $BiOCl_{0.75}Br_{0.25}$ material[4].The XPS signal of Cl 2p (Fig. 3d) fitted with the peak at binding energy of 198.13 eV and 199.75eV were characteristic for

Cl^- anions in Bi-Cl and C-Cl, separately. Fig. 3e showed that the XPS spectrum for the O 1s region was matched with two peaks at 532.0 and 530.2 eV. The main peak at 532.0 eV was related to the Bi-O bonds in $[Bi_2O_2]$ slabs of BiOX layered structure. The peak centered at 530.2 eV was assigned to the oxygen-containing groups (hydroxyl groups or water molecules adsorbed on the surface of the sample)[33]. Generally, the C1s core-level spectra of GO can be devolved into three peaks: (a) the non-oxygenated sp^2 bonded carbon at 284.5 eV, (b) the carbon in epoxy/hydroxyls (C-O) at 286.2 eV, and (c) the carbonyl carbon (C=O) at 288.4 eV[34, 35]. In the XPS spectrum of C1s from BG5.0 (Fig. 3f), the oxygenated functional groups decreased markedly and the distinct peak at 284.5 eV corresponding to graphitic carbon were prominent, confirming the deoxygenation of GO during the solvothermal synthesis process. All the characterizations above indicated the successful combination of $BiOCl_{0.75}Br_{0.25}$ and graphene in the products. $BiOCl_{0.75}Br_{0.25}$ microspheres were achieved with the aid of CTAB and CTAC, which served as bromide and chloride suppliers and also as structure-directing agents[16]. Meanwhile, the reduction of GO and the assembly precipitation of the $BiOCl_{0.75}Br_{0.25}$ on graphene were successfully completed. They firmly contacted with each other with the new chemical bonds formed during the hydrothermal reduction, such as Bi-C, C-Cl verified by XPS.

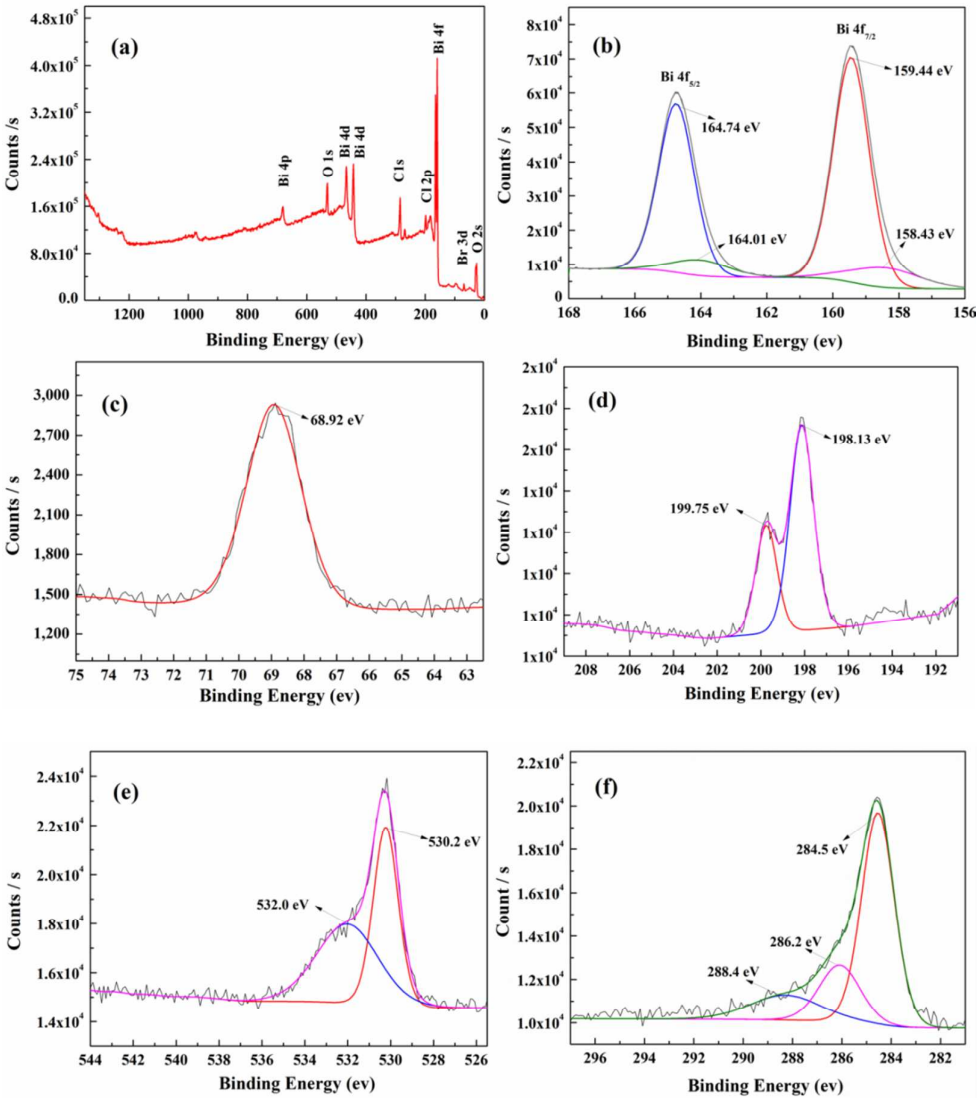

Fig.3. XPS spectra of BG5.0: (a) survey spectrum, (b) Bi 4f, (c) Br 3d, (d) Cl 2p, (e) O 1s and (f) C 1s.

3.2 Optical Properties of the samples

Fig. 4a displayed the UV-vis DRS of the pure $BiOCl_{0.75}Br_{0.25}$ and the BG hybrids. Compared to the pure $BiOCl_{0.75}Br_{0.25}$, BG hybrids exhibited a strong absorption in both UV and visible range. This phenomenon can be explained by the fact that the introduced graphene might act as photosensitizer chemically bonded with

$BiOCl_{0.75}Br_{0.25}$ and thus contribute to the visible light absorption. The optical absorption near the band edge followed the formula:

$$\alpha h\nu = \mathrm{A}(h\nu - \mathrm{E_g})^{n/2} \quad (1)$$

Where α, v, E_g and A were absorption coefficient, light frequency, band gap energy, and a constant, respectively. Among them, n was determined by the type of optical transition of a semiconductor (n = 1 for direct transition and n = 4 for indirect transition) [36]. The E_g of the as-prepared samples can be calculated from a plot depicting $(\alpha h\ v)^{1/2}$ versus $(h\ v)$, as shown in Fig.4b. The band gap energies (E_g values) of $BiOCl_{0.75}Br_{0.25}$, BG2.0, BG5.0 and BG10.0 were estimated to be 3.05, 2.02, 2.43 and 1.56 eV.

To further investigate the separation capacity of the photo-induced carriers in semiconductors, the PL spectra of the samples were obtained. Fig. S2 presented the PL spectra for pure $BiOCl_{0.75}Br_{0.25}$ and BG hybrids at an excitation wavelength of 404 nm. The PL spectrum of pure $BiOCl_{0.75}Br_{0.25}$ showed a strong emission. However, with the introduction of graphene, the emission intensity of the BG photocatalysts significantly decreased, with the BG5.0 sample having the weakest intensity. The result indicated that the efficient transfer of photo-induced electrons between $BiOCl_{0.75}Br_{0.25}$ and graphene facilitated the electron-hole separation, and thus improves the photocatalytic activity.

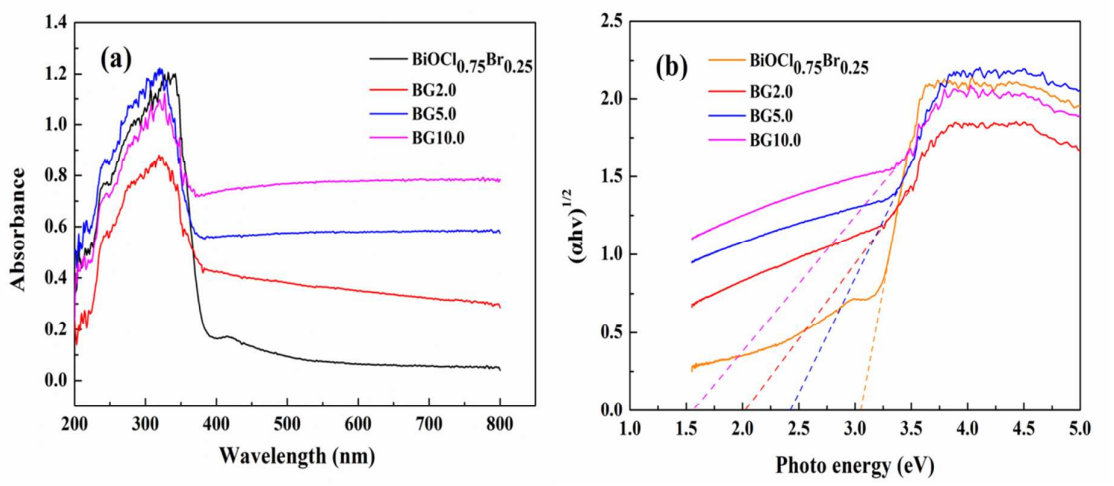

Fig.4. (a) UV–vis diffuse reflectance spectra of the samples; (b) the band gaps (Eg) of different samples.

3.3 N_2 sorption isotherms

The ability of photocatalysts to adsorb target pollutants was another noticeable factor in affecting its photocatalytic performance. The specific surface area and porosity of $BiOCl_{0.75}Br_{0.25}$ and BG5.0 were investigated by using nitrogen adsorption and desorption isotherms (as shown in Fig. 5). The isotherms can be categorized as type IV with a distinct hysteresis loop observed in the range of 0.4-1.0 p/p_0, implying the presence of mesopores in the size range of 2-50 nm[37]. The corresponding porosity distribution of the samples was shown in the insets of Fig. 5.The average pore diameter was calculated to be 5.946nm and 4.868 nm for $BiOCl_{0.75}Br_{0.25}$ and BG5.0. The Brunauer–Emmett–Teller (BET) surface areas of the samples calculated from N_2 isotherms were 20.26 $m^2 g^{-1}$ and 35.0 $m^2 g^{-1}$, respectively .Such mesoporous architecture and the larger surface area of BG5.0 played an important role in the adsorption process and the catalyst reaction.

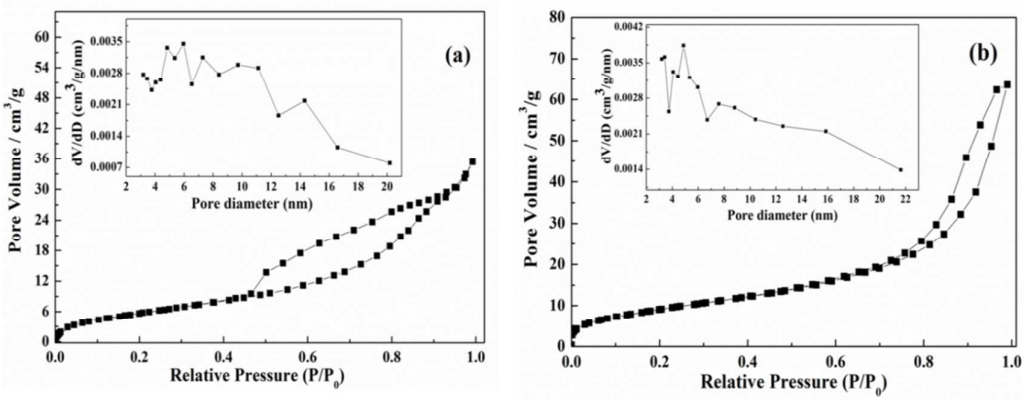

Fig.5. N_2 adsorption and desorption isotherms of the (a) $BiOCl_{0.75}Br_{0.25}$ (b) BG5.0.Insets: the corresponding pore-size distribution.

3.4 Photocatalytic activity of RhB under visible lights

To determine the photocatalytic activity of the as-prepared samples, the degradation of RhB was investigated under visible light irradiation. Fig. 6a presented the variation of the RhB concentration (C/C_0) as a function of the irradiation time over BG photocatalysts. The dark experiment with no significant changes confirmed that the adsorption-desorption equilibrium can be achieved after 60 min stirring at dark. As shown in Fig. 6a, BG2.0, BG5.0, and BG10.0 could remove 94.7%, 97.8%, and 91.2% of RhB which were better than the pure $BiOCl_{0.75}Br_{0.25}$. The temporal evolution of the spectral changes of the RhB mediated by the samples was also detected (Fig. S3, Supporting Information).

To quantitatively understand the reaction kinetics of the RhB degradation, the pseudo-first-order kinetics model was used to fit the photodegradation data, the equation is:

$$-\ln(C_t/C_0) = \mathrm{kt} \quad (5)$$

Where k (min^{-1}) and t (min) were the apparent first-order rate constant and irradiation time, C_0 (mg/L) and C_t (mg/L) were the initial concentration of RhB and the remaining concentrations of RhB at each time, respectively [38-40]. The model fitting plots and corresponding k values were shown in Fig. 6c and Fig. 6d. The initial removal constants were calculated to be 0.068, 0.118, 0.151, and 0.098 min^{-1} for $BiOCl_{0.75}Br_{0.25}$, BG2.0, BG5.0, and BG10.0, respectively.

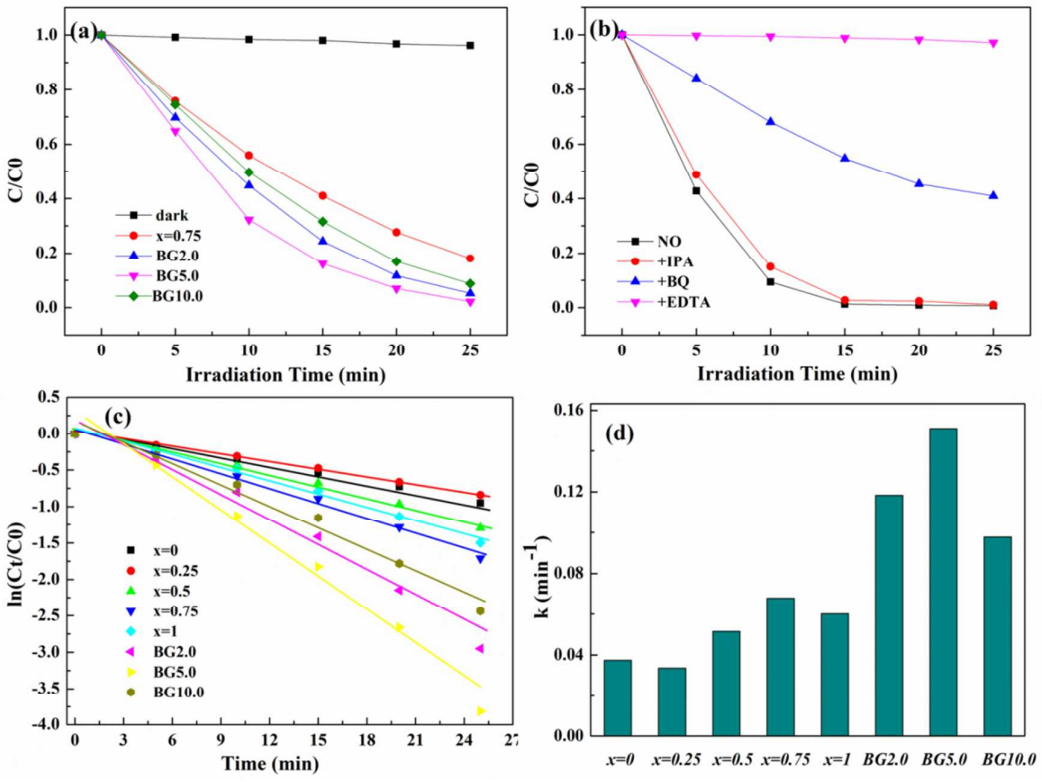

Fig.6. (a) Photocatalytic degradation of RhB over $BiOCl_{0.75}Br_{0.25}$/graphene composites under visible light (λ≥420 nm) irradiation; (b) Photocatalytic degradation of RhB (100ml, 50ppm) with BG5.0 in the absence and presence of different scavengers.(c) pseudo first-order kinetics fitting plots and (d) apparent first-order rate constants for various photocatalysts.

The result suggested that the introduction of graphene can efficiently enhance the photocatalytic performance of $BiOCl_{0.75}Br_{0.25}$. This may be ascribed to the increased active adsorption sites and photocatalytic reaction centers offered by graphene. Besides, graphene can act as an electronic "high way" and decrease the recombination of the photoexcited electron-hole pairs. BG5.0 showed the highest RhB removal efficiency (97.8%). However, a further increase in graphene amount (10wt %) led to a decrease in photocatalytic efficiency of the composite. The reason was that the excessive graphene could act as a kind of recombination center and promote the recombination of electron-hole pairs in graphene (Fig. S2, Supporting information)[34]. Additionally, the large of black may weaken the intensity of light through the depth of the reaction solution, which would lead to a decreased photocatalytic activity[41, 42] .

In addition, as illustrated in Fig. 7, the by-products in aqueous solution after photocatalytic reaction were further analyzed by HPLC. Obviously, some incomplete mineralized intermediates of RhB formed during the irradiation process, which was answerable for the blue shift of the absorption peak (Fig. S3, Supporting Information).The intensity of RhB peak decreased quickly while the concentration of other intermediates first increased and subsequently decreased with further irradiation. It was generally reported that the decomposition was mainly a de-ethylated process[36, 43]. In addition to RhB, five intermediates were evidently observed (Fig.7 b). The result may correspond to the N-deethylated products during the de-ethylated process. Namely, N,N-diethyl-N′-ethylrhodamine (DER), N-ethyl-N'-ethylrhodamine (EER), N, N-diethylrhodamine (DR), N-ethylrhodamine (ER), and rhodamine (R) ,

corresponded to peaks b-f, respectively[44, 45].Then, the conjugated structure of RhB was assault and some organic acidic molecules were produced due to the process of opening-ring[46, 47]. Finally, these organic acidic molecules were further mineralized to water and carbon dioxide. On the basis of the above results, one rational pathway for the visible light induced photocatalytic degradation of RhB was put forward and depicted in Fig. 8.

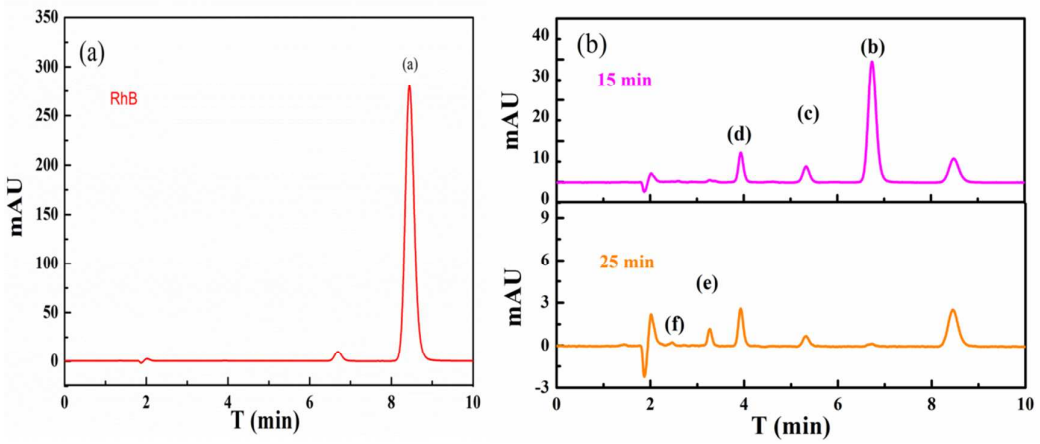

Fig.7. HPLC chromatograms of the RhB and the N-deethylated intermediates recorded at 554 nm at 15 and 25 m

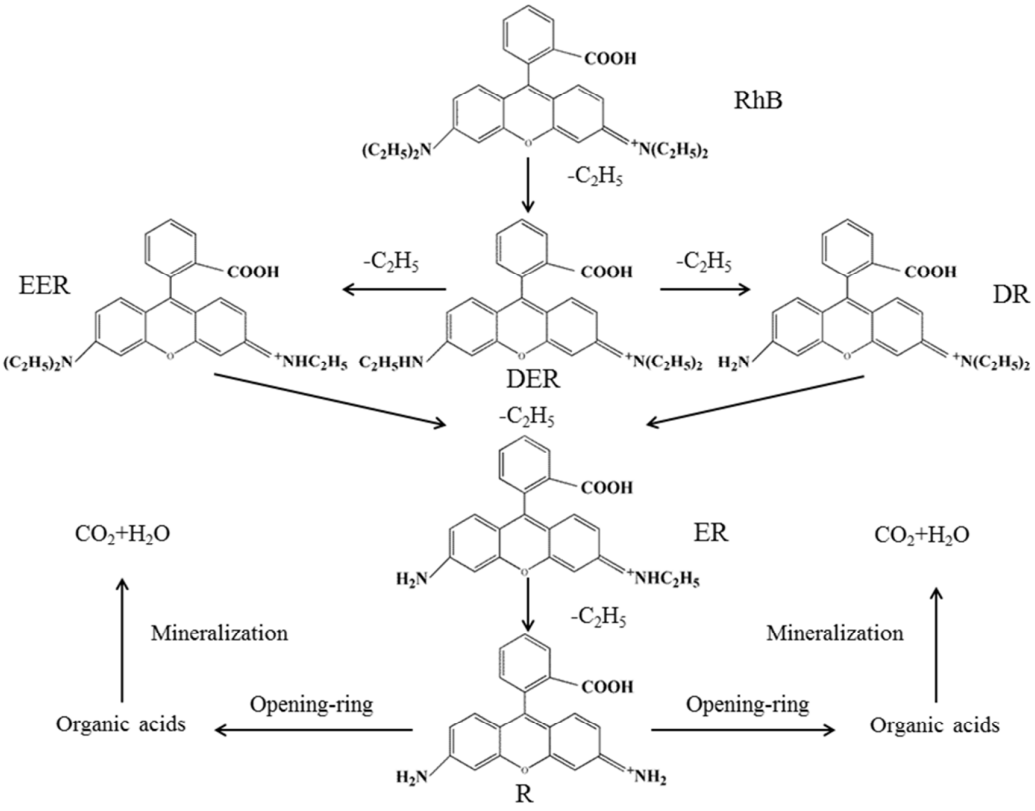

Fig. 8. Proposed pathway for the photocatalytic degradation of RhB dye under visible light.

3.4.1 Major active species and photocatalytic mechanism

The photodegradation of organic pollutants may involve one or more of the reactive species $^{\cdot}OH$, h^+, and $^{\cdot}O_2^{-}$[11]. An alternative chemical method by adding scavengers was used to investigate the role of the active species in the disintegration of RhB. Isopropyl alcohol (IPA), benzoquinone (BQ) and EDTA as scavengers for $^{\cdot}OH$, $^{\cdot}O_2^{-}$and h^+ were dissolved in the reaction solution, respectively[14, 40]. Fig. 6b displayed photodegradation of BG5.0 for RhB upon addition of various scavengers. Apparently, the RhB degradation was almost totally suppressed after trapping h^+ by

adding EDTA. BQ ($\cdot O_2^-$scavenger) also appeared significantly suppressed on the dye degradation. However, IPA acted as $\cdot OH$ trapping agent presented no influence on photoactivity.

On the basis of the aforementioned results and analysis, a possible mechanism was proposed as Scheme 1 to explain the process of BG5.0 removing RhB under visible light irradiation.

$$BiOCl_{0.75}Br_{0.25} + \text{visible light} \rightarrow BiOCl_{0.75}Br_{0.25}(e_{CB^-} + h_{VB^+}) \quad (1)$$

$$BiOCl_{0.75}Br_{0.25}(e_{CB^-}) + \text{graphene} \rightarrow \text{graphene}(e_{CB^-}) \quad (2)$$

$$e_{CB^-} + \text{adsorbed } O_2(\text{surface O}) \rightarrow \cdot O_{2^-} \quad (3)$$

$$H_2O + BiOCl_{0.75}Br_{0.25}(h_{VB^+}) \rightarrow H^+ + \cdot OH \quad (4)$$

$$\cdot O_{2^-} + H^+ \rightarrow \cdot OH \quad (5)$$

$$OH^- + BiOCl_{0.75}Br_{0.25}(h_{VB^+}) \rightarrow \cdot OH \quad (6)$$

$$h^+, \cdot O_{2^-} + \text{adsorbed dye/dye}^+ \rightarrow \text{degradation products} \quad (7)$$

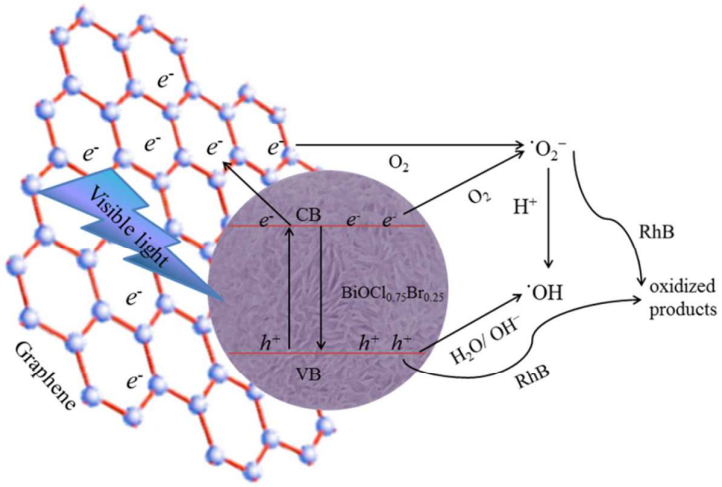

Scheme 1. The photocatalytic mechanism of RhB over BG composites.

Once the material was irradiated, the electrons (e_{CB}-) can be excited to the conduction band (CB) from the valence band (VB) of the $BiOCl_{0.75}Br_{0.25}$, leaving

behind a hole in the valence band simultaneously. Then, graphene accepted the photogenerated electrons from $BiOCl_{0.75}Br_{0.25}$ and transported apace to separate the photogenerated electron-hole pairs. The flow electrons accumulated on the surface of graphene could be captured by the surface-absorbed molecular (or atomic) oxygen to yield $\cdot O_2^-$. The superoxide radical anion acted as an oxidant to attack the pollutants and the pollutants were degraded gradually[38]. The activated $\cdot O_2^-$ further proceeded to form active $\cdot OH$ radicals via a series of reaction with H^+. The adsorbed OH^- species may also capture the hole to form $\cdot OH$ radicals [36]. However, the $\cdot OH$ radical did not participated in the dye degradation since there was no $\cdot OH$ scavenger effect. To summarize, the $\cdot O_2^-$ and h^+ as dominant active species undergo the main responsibility to degrade the dye.

3.4.2 Stability of the catalyst

Reuse activity was an important parameter for photocatalytic materials. According to the experimental data, BG5.0 showed the highest photocatalytic activity. Thus, BG5.0 was selected as model and undergone the cycling tests. Four circulating runs in the photocatalytic decomposition of RhB under visible light were checked iteratively under the same trace. As can be seen from Fig. 9, even after four recycles for the photodegradation of RhB, the degradation ratio of RhB can still reach near 90%. Notably, there was no distinction between the XRD results before and after the reaction (Fig.10). The results indicated that the BG5.0 possessed good photocatalytic stability, which was principal for its industrial applications.

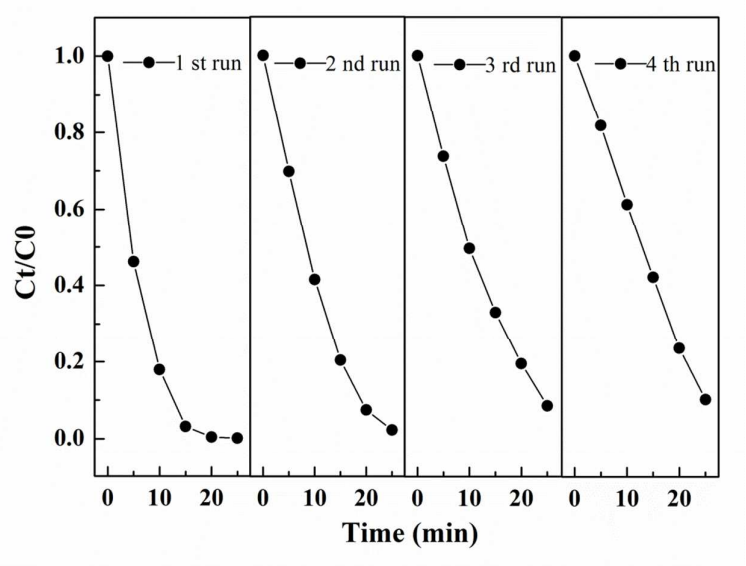

Fig. 9. Recycling test of BG5.0 in photocatalytic degradation of RhB.

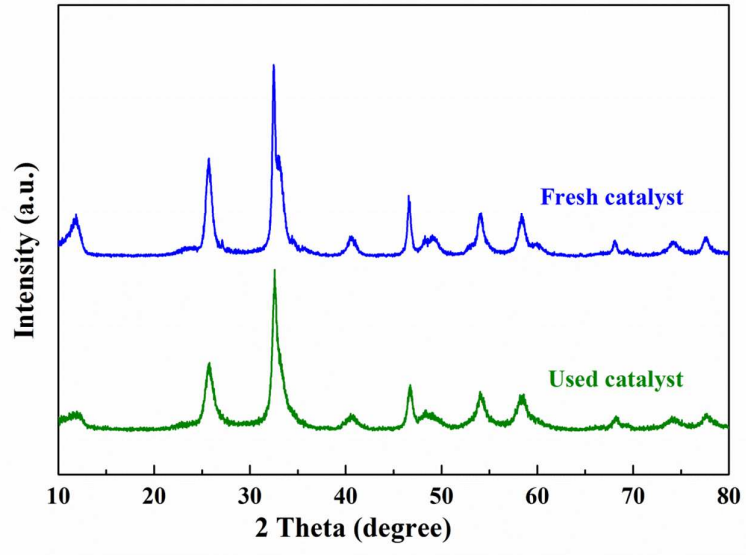

Fig. 10. The XRD patterns of BG5.0 catalyst: a) fresh catalyst and b) used catalyst.

4. Conclusions

3D $BiOCl_{0.75}Br_{0.25}$/graphene had been synthesized by a facile solvothermal route and the photocatalytic activities of them were evaluated by the photodegradation of RhB. The BG photocatalysts exhibited a higher photocatalytic activity than pure $BiOCl_{0.75}Br_{0.25}$, and the activity was almost up to 2.3 times when loaded with 5.0 wt% graphene. The enhanced photoactivity can be attributed to t the effective light absorption, the larger specific surface areas and the more efficient charge transportations and separations. The introduced graphene acted as an electron collector and transporter to separate photogenerated electron-hole pairs. $\cdot O_2^-$ and h^+ as dominant active species generated during the photocatalytic process were ordered to attack the pollutants. Furthermore, the design of alloyed compounds and graphene composites enlightened more possibility about the potential application of graphene-based materials in the field of wastewater treatment.

Acknowledgments

The authors gratefully acknowledge the financial support provided by Collaborative Innovation Center of Resource–Conserving & Environment-friendly Society and Ecological Civilization, the Hunan Province Innovation Foundation for Postgraduate (No. CX2014B142), the National Natural Science Foundation of China (No. 71431006).

Reference

1. Chen, C.; Ma, W.; Zhao, J., *Chem. Soc. Rev,* 2010, **39**, 4206-4219.

2. Zhang, X.; Ai, Z.; Jia, F.; Zhang, L., *J. Phys. Chem. C,* 2008, **112**, 747-753.

3. Zhang, L.; Cao, X. F.; Chen, X. T.; Xue, Z. L., *J. Colloid. Interface. Sci,* 2011, **354**, 630-636.

4. Huo, Y.; Zhang, J.; Miao, M.; Jin, Y., *Appl. Catal. B: Environ,* 2012, **111-112**, 334-341.

5. Zhu, L.-P.; Liao, G.-H.; Bing, N.-C.; Wang, L.-L.; Yang, Y.; Xie, H.-Y., *CrystEngComm* 2010, **12**, 3791-3796.

6. Hu, J.; Weng, S.; Zheng, Z.; Pei, Z.; Huang, M.; Liu, P., *J. Hazard. Mater,* 2014, **264**, 293-302.

7. Cao, J.; Xu, B.; Lin, H.; Luo, B.; Chen, S., *Chem. Eng. J,* 2012, **185-186**, 91-99.

8. Chang, X.; Gondal, M. A.; Al-Saadi, A. A.; Ali, M. A.; Shen, H.; Zhou, Q.; Zhang, J.; Du, M.; Liu, Y.; Ji, G., *J. Colloid. Interface. Sci,* 2012, **377**, 291-298.

9. Wei, X. X.; Cui, H .; Guo, S.; Zhao, L.; Li, W., *J. Hazard. Mater,* 2013, **263**,650-658.

10. Sudeep, P. M.; Narayanan, T. N.; Ganesan, A.; Shaijumon, M. M.; Yang, H.; Ozden, S.; Patra, P. K.; Pasquali, M.; Vajtai, R.; Ganguli, S.; Roy, A. K.; Anantharaman, M. R.; Ajayan, P. M. *Acs Nano* 2013, **7**, 7034-7040.

11. Jiang, S.; Zhou, K.; Shi, Y.; Lo, S.; Xu, H.; Hu, Y.; Gui, Z., *Appl. Surf. Sci,* 2014, **290**, 313-319.

12. Jiang, G.; Li, X.; Wei, Z.; Jiang, T.; Du, X.; Chen, W., *Powder Technol,* 2014, **260**,

84-89.

13. Lu, L.; Kong, L.; Jiang, Z.; Lai, H. H. C.; Xiao, T.; Edwards, P. P., *Catal.Lett,* 2012, **142**, 771-778.

14. Kim, W. J.; Pradhan, D.; Min, B.-K.; Sohn, Y., *Appl. Catal. B: Environ,* 2014, **147**, 711-725.

15. Lei, Y.; Wang, G.; Guo, P.; Song, H., *Appl. Surf. Sci,* 2013, **279**, 374-379.

16. Gnayem, H.; Sasson, Y., *ACS Catal,* 2013, **3**, 186-191.

17. Ai, Z.; Ho, W.; Lee, S., *J. Phys. Chem. C,* 2011, **115**, 25330-25337.

18. Wang, H.; Yuan, X.; Wu, Y.; Chen, X.; Leng, L.; Wang, H.; Li, H.; Zeng, G., *Chem. Eng. J,* 2014, doi: http://dx.doi.org/10.1016/j.cej.2014.10.020

19. Wang, H.; Yuan, X.; Wu, Y.; Huang, H.; Zeng, G.; Liu, Y.; Wang, X.; Lin, N.; Qi, Y., *Appl. Surf. Sci,* 2013, **279**, 432-440.

20. Wu, Z.; Zhong, H.; Yuan, X.; Wang, H.; Wang, L.; Chen, X.; Zeng, G.; Wu, Y., *Water res,* 2014, **67C**, 330-344.

21. Dong, S.; Hu, L.; Feng, J.; Pi, Y.; Li, Q.; Li, Y.; Liu, M.; Sun, J.; Sun, J., *RSC Adv,* 2014, **4**, 64994-65003.

22. Wu, Y.; Luo, H.; Wang, H., *RSC Adv,* 2014, **4**, 40435-40438.

23. Xiao, F.-X.; Miao, J.; Liu, B., *J. Am. Chem. Soc,* 2014**, 136**, 1559-1569.

24. Xiang, Q.; Lang, D.; Shen, T.; Liu, F., *Appl. Catal. B-Environ,* 2015**, 162**, 196-203.

25. Yang, X.; Cui, H.; Li, Y.; Qin, J.; Zhang, R.; Tang, H., *Acs Catal,* 2013**, 3**, 363-369.

26. Yang, X.; Qin, J.; Li, Y.; Zhang, R.; Tang, H., *J. Hazard. Mater,* 2013**, 261**, 342-350.

27. Qiu, B.; Xing, M.; Zhang, J., *J. Am. Chem. Soc,* 2014, **136**, 5852-5855.

28. Liu, Y.; Son, W. J.; Lu, J.; Huang, B.; Dai, Y.; Whangbo, M. H., Chemistry 2011, **17**, 9342-9349.

29. Yan, J.; Wang, K.; Liu, Q.; Qian, J.; Dong, X.; Liu, W.; Qiu, B., *RSC Adv,* 2013, **3**,14451-14457.

30. Cui, W.; Ma, S.; Liu, L.; Hu, J.; Liang, Y.; McEvoy, J. G., *Appl. Surf. Sci,* 2013, **271**, 171-181.

31. Liu, J.-Y.; Bai, Y.; Luo, P.-Y.; Wang, P.-Q., *Catal. Commun,* 2013, **42**, 58-61.

32. Gao, F.; Zeng, D.; Huang, Q.; Tian, S.; Xie, C., *Phys. Chem. Chem. Phys,* 2012, **14**, 10572-10578.

33. Liu, Z.; Xu, W.; Fang, J.; Xu, X.; Wu, S.; Zhu, X.; Chen, Z., *Appl. Surf. Sci,* 2012, **259**, 441-447.

34. Song, S.; Gao, W.; Wang, X.; Li, X.; Liu, D.; Xing, Y.; Zhang, H., *Dalton trans,* 2012, **41**, 10472-10476.

35. Liu, H.; Su, Y.; Chen, Z.; Jin, Z.; Wang, Y., *J. Hazard. Mater,* 2014, **266**, 75-83.

36. Jia, Z.; Wang, F.; Xin, F.; Zhang, B., *Ind. Eng. Chem. Res,* 2011, **50**, 6688-6694.

37. Li, Y.; Wang, J.; Yao, H.; Dang, L.; Li, Z., *J. Mol. Catal. A: Chem,* 2011, **334**, 116-122.

38. Liu, H.; Cao, W. R.; Su, Y.; Chen, Z.; Wang, Y., *J. Colloid. Interface. Sci,* 2013, **398**, 161-167.

39. Soltani, T.; Entezari, M. H., *Chem. Eng. J,* 2013, **223**, 145-154.

40. Liu, J.; Li, H.; Du, N.; Song, S.; Hou, W. G., *RSC Adv,* 2014, **4** , 31393-31399.

41. Li, Q.; Guo, B.; Yu, J.; Ran, J.; Zhang, B.; Yan, H.; Gong, J. R., *J. Am. Chem. Soc,* 2011, **133**, 10878-10884.

42. Zhang, Y.; Tang, Z.-R.; Fu, X.; Xu, Y.-J., *Acs Nano* 2010, **4**, 7303-7314.

43. Shenawi-Khalil, S.; Uvarov, V.; Kritsman, Y.; Menes, E.; Popov, I.; Sasson, Y., *Catal. Commun,* 2011, **12**,1136-1141.

44. Yu, K.; Yang, S.; He, H.; Sun, C.; Gu, C.; Ju, Y., *J. Phys. Chem. A,* 2009, **113**, 10024-10032.

45. Fu, H.; Zhang, S.; Xu, T.; Zhu, Y.; Chen, J., *Environ. Sci. & technol,* 2008, **42,** 2085-2091.

46. Natarajan, T. S.; Thomas, M.; Natarajan, K.; Bajaj, H. C.; Tayade, R. J., *Chem. Eng. J,* 2011, **169**, 126-134.

47. He, Z.; Sun, C.; Yang, S.; Ding, Y.; He, H.; Wang, Z., *J. Hazard. Mater,* 2009, **162**, 1477-86.